iEMSs 2008: International Congress on Environmental Modelling and Software
Integrating Sciences and Information Technology for Environmental Assessment and Decision Making
4th Biennial Meeting of iEMSs, http://www.iemss.org/iemss2008/index.php?n=Main.Proceedings
M. Sànchez-Marrè, J. Béjar, J. Comas, A. Rizzoli and G. Guariso (Eds.)
International Environmental Modelling and Software Society (iEMSs), 2008

Mud-flow and lava-flow susceptibility and hazard mapping through numerical modelling, GIS techniques, historical and geo-environmental analyses

Giulio Iovine
CNR-IRPI via Cavour, 6 – 87036 Rende (CS) ITALIA (g.iovine@irpi.cnr.it)

Abstract: A method for mapping mud flows and lava flows, and for evaluating related susceptibility and hazard has recently been tested at different study areas of Southern Italy (located in Campania, Calabria, and Sicily), which have repeatedly been affected by damaging events in historical time. The approach is based on numerical models, GIS-techniques, geo-environmental and historical evaluations. Results have been obtained through a statistical approach by simulating a large number of events on a cluster. Employed cellular automata models have first been calibrated, either manually (by trial and error) or by means of Genetic Algorithms, and then validated against past flow events that occurred in the same study areas, or in similar geo-environmental settings. Simulations have been quantitatively evaluated with respect to real cases by means of two distinct functions of fitness based on 1) the affected areas for mudflows, and on 2) affected areas and duration for lava flows. Aiming at susceptibility/hazard assessment, a grid of possible sources has been hypothesised on the basis of historical/geological knowledge and statistics of past events. For each source, a high number of simulations has been planned by adopting combinations of sources' and materials' characteristics. Probabilities of activation, empirically based on past events, have been assigned to each source of the grid by considering its location and geological information. Different probabilities have also been assigned to each "type of event" by taking into account their observed historical frequencies. Two different types of maps were realized in a GIS: 1) a susceptibility map, realised by simply counting the frequencies of flows affecting each site; 2) a hazard map, in which probabilities have been "empirically" attributed to each simulation based on location of sources and types of event. Preliminary results (based on a subset of the overall planned simulations) clearly depict the most susceptible and hazardous sectors.

Keywords: Lava flows; Mud flows; Modelling & Simulation; Susceptibility; Hazard.

1. INTRODUCTION

In so far as mud flows and lava flows are considered, hazard mapping procedures require - besides the usual prediction of time of occurrence and of source location - the assessment of the travel distance (run out), or better the area affected by the propagation of the initial event and of its energetic characteristics. For these types of phenomena, hazard mapping procedures are sometimes based on empirical geological reasoning, or they depend on either empirical-statistical evaluations or statistical-probabilistic analyses of past events [cf. D'Ambrosio et al., 2007; Crisci et al., in press - and references therein]. Available approaches are usually distinguished into deterministic and probabilistic methods, or a combination of both techniques.
Modelling and simulation represent a valuable tool for hazard evaluation. By employing such techniques, the timely simulation of the possible flow paths and the evaluation of the effects of planned remedial/control works on the behaviour of future events could profitably be carried out. Following Hungr [1995], any simulation model should be easy to

calibrate through back-analyses against real cases; it should describe the essential characteristics of the phenomenon, allowing also for simulating flow branching and rejoining; it should not suffer from mesh-related problems. As concerns model reliability, one possible approach of evaluation relies on thorough calibration and successive validation by considering a sufficient number of case studies. Sensitivity analyses may further help in evaluating the role of model parameters, mesh geometry and quality of input data on the model behaviour [cf. e.g. D'Ambrosio et al., 2007]. Ideally, a multiphase 3D model of material which moves over a complex topography would be an optimal choice for accurate assessment. However, this type of model generally requires large computational power and a number of parameters which may demand considerable efforts for calibration. Moreover, they generally suffer from instability problems and commonly need site-specific settings. A proper but simplified approach would seem appropriate.
In the past decades a variety of numerical models were successfully developed for simulating various types of gravity flows [e.g. Crisci et al., 1982; Murray and Paola, 1994; Miyamoto and Sasaki, 1997; Iverson et al., 1998; Di Gregorio and Serra, 1999; D'Ambrosio et al., 2001; Iovine and Di Gregorio, 2003; Pitman et al., 2003]. Within the frame of parallel computing, Cellular Automata (CA) models are able to simulate complex systems, which can be described in terms of local interactions. Well known CA examples are Lattice Gas Automata and Lattice Boltzmann models [cf. Succi, 2004], which are particularly suitable for modelling fluid dynamics at a microscopic scale. However, many natural phenomena – and, among these, gravity flows - generally affect quite large areas and need a macroscopic level of description. Standard approaches based on differential equations [cf. McBirney and Murase, 1984; Iverson, 1997 – and many others] may suffer in capturing the essential features of the phenomena to be simulated; employed equations are commonly rather complex and involve adoption of approximated numerical methods of solution. In such cases, Macroscopic Cellular Automata (MCA) represent a suitable alternative [Di Gregorio and Serra, 1999].
Analyses of lava-flow and mud-flow susceptibility/hazard have recently been started in separate study areas of Southern Italy, by employing MCA models combined with GIS techniques [e.g. Iovine et al., 2003a, b; Crisci et al., in press]. Historical and geo-environmental analyses, aimed at quantitatively evaluating return periods of considered event types are presently in progress, as well as part of the overall planned simulations. In the following only preliminary results are therefore briefly described, with reference to 1) lava flows on the SE flank of Mount Etna (Sicily), and to 2) mud-flows on the southern slope of the Pizzo d'Alvano Massif and in the San Martino Valle Caudina-Cervinara area (Campania). Finally, an example of susceptibility zonation is also reported for another sector, located along the southern Tyrrhenian coast of Calabria between the villages of Bagnara and Scilla, not far from the Messina Strait.

2. THE STUDY AREAS

Among the study areas considered for lava-flow hazard analyses, one is located on the SE flank of Mt. Etna, the largest sub-aerial active volcano of Europe (Figure 1). Etna is composed of several nested strato-volcanoes plus scattered eruptive centres, which opened through a basement of tholeiitic/transitional fissural basalts dating back to 500 ky BP. The volcanic basement overlies Middle-Late Pleistocene sediments covering the Maghrebian-Apennine Chain (CNR, 1979). The dominant type of Etnean activity is effusive. In historical times, the eastern flank of the volcano was frequently affected by lava flows originating from flank eruptions [e.g. Romano and Sturiale, 1982], either through lateral fractures or eccentric vents. From a structural point of view, two main "weakness zones" are to be found by the volcano summit: the "N-S Rift" and the "NE Rift". Moreover, a high spatial density of fractures, effusive fissures and pyroclastic cones characterizes the eastern flank of the volcano [Behncke et al., 2005], mainly along a SSE-trending fracture system which crosses the study area between the villages of Nicolosi and Trecastagni [Corazzato and Tibaldi, 2006]. Finally, a dormant deep-seated gravitational sliding (DGSD) towards the Jonian Sea, associated with a larger volcano-tectonic phenomenon, affects the whole south-eastern flank of the volcano [Borgia et al., 1992]. The margins of the DGSD are marked by the mentioned major weakness zones: its right flank crosses the study area and

corresponds to the "transitional" weakness zone which connects the N-S Rift to the transtensional fault system marked by the Trecastagni and Mascalucia faults.

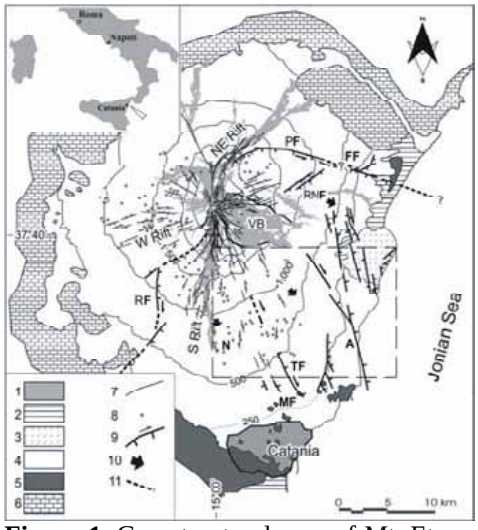

In the map on the left, the study area is shown by a dashed rectangle. Symbols and grey tones have the following meanings: 1) 1900-2002 lava flows; 2) recent alluvial deposits; 3) deposits resulting from the emptying of Valle del Bove; 4) Etnean volcanics; 5) Early Quaternary clays; 6) Pre-Quaternary sediments; 7) main eruptive fractures; 8) pyroclastic cones; 9) main faults; 10) direction of displacement of either the DGSD or the volcano-tectonic phenomenon; 11) boundaries of the unstable sector; FF) Fiumefreddo Fault; MF) Mascalucia Fault; PF) Pernicana Fault; RF) Ragalna Fault; RNF) Ripe della Naca Fault; TF) Trecastagni Fault; A) Acireale; N) Nicolosi; VB) Valle del Bove.

Figure 1. Geo-structural map of Mt. Etna - after Acocella and Neri [2003], mod.

As far as "mudflows" [*sensu* United Nations, 1997] are concerned, the first study area is located in the Caudina Valley on the northern slope of Mt. Pizzone, which belongs to the Partenio-Monti di Avella massif (blue rectangle in Figure 2). Still in the same region, the second study area is located about 15 km east of Mt. Vesuvius, on the southern slope of Mt. Pizzo d'Alvano, belonging to the Monti di Sarno massif (red rectangle in Figure 2).

Mesozoic carbonate rocks constitute the backbone of both the massifs, which are bounded by steep slopes cut along major tectonic elements. The bedrock is overlain by a regolith of residual and colluvial soils, mainly derived from Quaternary pyroclastic materials of the Somma–Vesuvius volcanic complex and of the Phlegrean Fields. The thickness of the regolith, and its geotechnical properties vary widely from site to site. At the base of the massifs, thick colluvial and alluvial deposits mark the transition to the alluvial plains; here, at the mouth of the main drainages, voluminous debris fans are to be found. Several villages with their related infrastructures are to be found in the transitional sector at the base of the massifs.

Figure 2. Geological map of the study areas in Campania - after Del Prete et al. [1998], mod. Key: (1) alluvial sediments; (2) pyroclastic terrains (a) and lavas (b); (3) clay, marl and sandstone; (4) carbonate; (5–7) isopleths (in cm) of the Somma-Vesuvius air-fall deposits of year 1800 B.C. (5), 79 A.D. (6) and 472 A.D. (7).

At Pizzo d'Alvano, hundreds of soil slip-debris flows were triggered by heavy rains on 5–6 May 1998 [Del Prete et al., 1998], severely inundating the villages of Sarno, Siano, Bracigliano and Quindici (and causing 161 deaths). In the Caudina Valley, the villages of Cervinara and San Martino V.C. were particularly affected by the soil slip-debris flows triggered by the meteoric event of 15–16 December 1999 [Vittori et al., 2000].

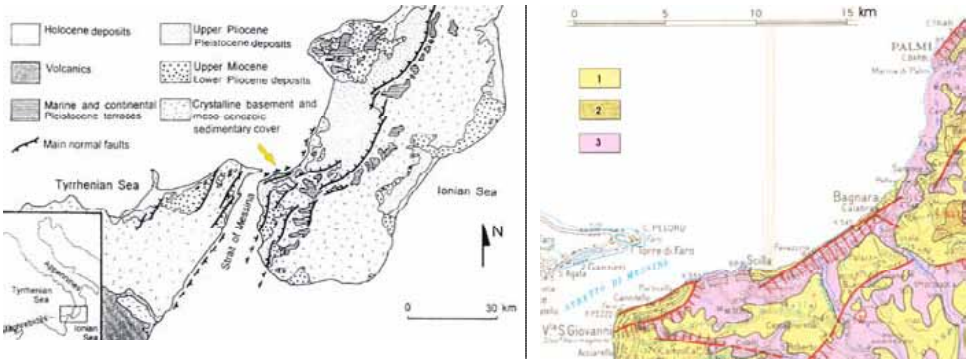

Figure 3. Geological sketches of the Calabrian study area. a) On the left, a geological map (location marked by the yellow arrow) - after Tortorici et al. [1995], mod. b) On the right, a litho-structural map. Key: 1) terraced sand, clay, pebble (Quaternary); 2) sand, clay, and marl, with subordinate evaporite (Upper Miocene-Pliocene); 3) acid intrusive and middle-high grade metamorphic rocks of the Alpine continental nappe (Palaeozoic). In red, recent normal faults - after Sorriso-Valvo & Tansi [1996], mod.

Finally, the third study area for mud-flow susceptibility analyses is located in Calabria, between the villages of Bagnara Calabra and Scilla (Figure 3). This narrow strip of land along the southern Tyrrhenian coast is characterized by: notable slope energy in a terraced geomorphologic setting; short ephemeral streams with small watershed; high longitudinal gradients. Palaeozoic intrusive and metamorphic rocks that crop out along the coast and the main streams are overlain by Upper Miocene-Pliocene pelitic sediments and evaporites, which are in turn followed by Quaternary sediments. A recent NE-SW trending normal fault, which occurs along the coast, has a notable morphological evidence.
In the area, heavy rains frequently trigger soil slips on the steep slopes facing the sea; in the last 40 years, one event of single/multiple landslide activation occurred on the average every three years. The mobilized materials commonly became fluidized and ran towards the base of the slopes, damaging the villages and the major infrastructures (highway, state road SS.18, railway) located thereby. Among the recentmost damaging events, those that occurred on 12 May 2001 and on 31 March 2005 struck the hamlet of Favazzina and its surroundings, severely damaging (and interrupting) the cited infrastructures.

3. THE METHOD

Details concerning the models employed for simulating mudflows and lava flows can be found in D'Ambrosio et al. [2003a] and in Crisci et al. [2004], respectively, and will not be repeated here; the main characteristics of both models are listed in the Appendix. Likewise, the approach for mapping mud-flow susceptibility was first applied by Iovine et al. [2003a, b; 2007]; the method for lava-flow susceptibility and hazard mapping can be found in Crisci et al. [in press].
The model for simulating lava flows belongs to the family SCIARA of deterministic MCA models [Crisci et al., 1982]. The two-dimensional version *fv* [Crisci et al., 2004], based on a hexagonal tessellation of space, was used in this study. In *fv*, lava feeding is handled by specifying the cell/s that will act as vent/s; for this purpose an effusion-rate function has to be assigned to each vent. Lava flows among the cells are computed by applying the "minimisation algorithm of the differences" (cf. Appendix), proposed by Di Gregorio and Serra [1999]. Changes of lava temperature are modelled by means of the radiation equation, and lava viscosity varies accordingly. As a consequence of viscosity, the amount of lava which cannot flow out of the cell is computed (in terms of adherence). Finally, the halting of the lava flow depends on temperature: when it drops below a fixed threshold the thickness of lava is added to the cell elevation. The elementary processes included in the transition function σ of the model are: σ_1) lava outflows, σ_2) variation of lava temperature, and σ_3) lava halting.
Calibration was performed against the Etnean 2001 Mt. Calcarazzi eruption by employing parallel Genetic Algorithms (GA). Simulations were compared to real cases by means of the fitness function $e_{1t} = \sqrt{(e_1)^{t_1}(e_1)^{t_2}}$, defined in the interval [0,1] (where 1 corresponds

to perfect overlap), which takes into account both the areal extent of the real and simulated events, and their temporal duration. Note that, $e_1 = \sqrt{(R \cap S)/(R \cup S)}$ is the "basic" fitness function, which only compares the affected areas of the real (R) and simulated (S) events. Moreover, t_1 represents the duration of the real event, while $t_2 = t_1 + \Delta t$, where Δt is an arbitrary time increment. Validation was then performed against the 2002 Linguaglossa, and the 1991-93 Valle del Bove events, which are characterised by different durations, lava volumes, and effusion rates [cf. D'Ambrosio et al., 2006].

For susceptibility/hazard mapping purposes, a regular grid of hundreds of "possible" vents, located at 500 m intervals and uniformly covering the area, was hypothesised (Figure 4a). Aiming at pre-processing the simulation results, a sub-set of n.88 vents (located at 1 km intervals) was employed, allowing for the preliminary considerations discussed in the present paper. For each vent, a statistically-significant number of simulations was planned by adopting appropriate combinations of durations and lava volumes (Table 1), and effusion-rate functions (e.g. Figure 4c), which were selected on the basis of volcanological/historical knowledge. Accordingly, it was implicitly assumed that the volcanic style will not significantly change in the near future.

Performed simulations were stored in a GIS for susceptibility and hazard analyses. Maps for susceptibility evaluations were obtained by simply overlapping all the simulations; in other words, the same probability of occurrence was assigned to all types of events. By normalizing the obtained frequencies of events, five equal-interval classes of increasing "relative susceptibility" were distinguished and mapped by means of grey-tones (adopted ranges: 1=[0-0.2], 2=]0.2-0.4], 3=]0.4-0.6], 4=]0.6-0.8], 5=]0.8-1.0]).

As for hazard evaluations, historic and volcanological information on past eruptions was also taken into account. Probabilities of activation ($h_a = h_{elev} \cdot h_{wz} \cdot h_{df}$), empirically based on past behaviour of the volcano, were assigned to each vent of the grid by considering i) elevation (h_{elev} - Figure 4b), and ii) location with respect to the volcanic edifice (cf. Figure 5), and particularly the proximity to the main weakness zones (h_{wz}) and the spatial densities of eruptive fissures (h_{df}). Different probabilities ($h_e = h_{dv} \cdot h_{\gamma}$) were also assigned to the simulated eruption types, depending on combinations of durations and lava volumes (h_{dv}), and effusion-rate functions (h_{γ}). At any place affected by a given simulation (s_i), a value of hazard ($h_i = h_a \cdot h_e$) could be ascribed, depending on the conditioned probabilities of occurrence of that simulation. The overall hazard ($H_t = \sum h_i$) could be obtained by simply overlapping all the simulations in the GIS and by adding the related probabilities. Depending also on the number (n) of performed simulations, computed values ranged between two extremes; they were normalised and ranked the into five classes of "relative hazard" (H_r) - mapped in grey-tones (same ranges as for susceptibility).

Based on adopted criteria for probability evaluation, different maps of lava-flow hazard could be compiled [Crisci et al., in press]. In the example shown in the next section, a significant role was ascribed to the SSE-trending weakness zone on the right flank of the cited DSGD (cf. Figures 1 and 4). In more detail, h_{elev} was assigned by assuming a cubic relationship with vent elevation (cf. tendency line in Figure 4b, formula in caption), according to historical data [after Behncke et al., 2005]; h_{df} was set to 0.1, 0.3, and 0.6, respectively, depending on spatial density (ρ, number of vents per square km) of observed eruptive fissures and pyroclastic cones, which according to the same Authors can be distinguished into three classes ($\rho \leq 0.5$, $0.5 < \rho \leq 1$, and $\rho > 1$); h_{wz} assumed an "emphasising" role, by increasing by 30% values of activation probabilities of the vents located within its influence buffer (i.e. the weakness zone). Depending on possible combinations of h_{df} and h_{wz}, six classes of normalised activation probabilities resulted (see description of Figure 5).

Frequencies of historical eruptions were ranked into classes by durations and lava volumes, based on volcanological and historical data. Normalised probabilities (h_{dv}) for the types of event were derived from such frequencies (cf. Table 1, where only the types of eruption with shortest durations - considered in the present study - are listed). Finally, one single type of effusion-rate function was adopted for preliminary analyses (i.e. h_{γ} was ignored), characterized by a peak discharge at 1/3 of the eruption duration (cf. Figure 4c).

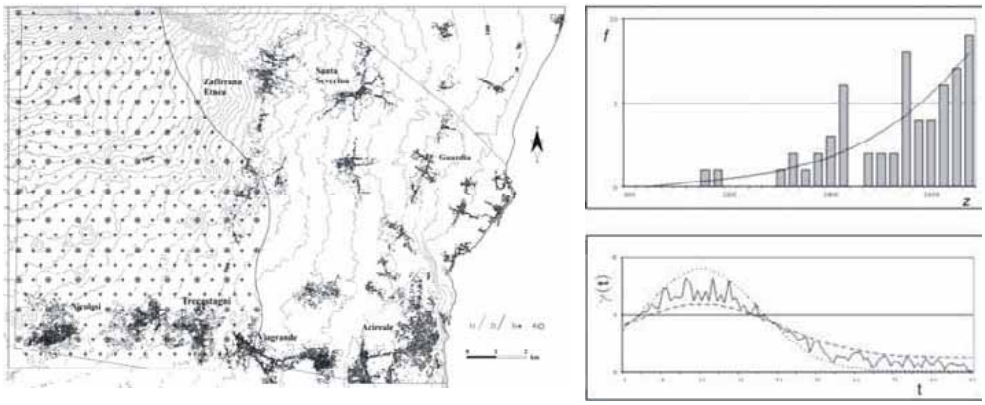

Figure 4. SE flank of Mt. Etna. a) On the left, grid of hypothesised vents. Key: 1) boundary of the study area; 2) eastern limit of the vents; 3) set of n.340 vents, located at 500 m intervals. 4) set of n.88 vents, at 1 km intervals. b) On top-right, relationship between number of historical lava flows (*f*) and elevation of the vents (*z*, in m a.s.l.). Tendency line is expressed by: $h_{elev} \propto 8 \cdot 10^{-10} \cdot z^3 + -2 \cdot 10^{-6} \cdot z^2 + 1.6 \cdot 10^{-3} \cdot z + 3.009 \cdot 10^{-1}$. c) On bottom-right, example of randomly-generated effusion-rate function: dotted lines define the variation range in which values were computed – after Crisci et al. [in press], mod.

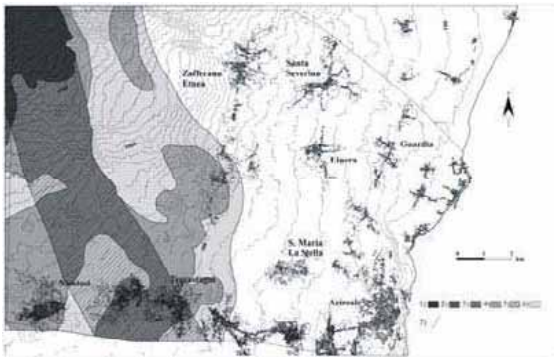

In the map on the left, the major SSE-trending weakness zone, which marks the right margin of the DGSD (cf. Figure 1), is shown by a dashed pattern. As far as locations of the vents are considered, the six classes of assumed probabilities ($h_{df} \cdot h_{wz}$) were normalised as follows: 1=0.34, 2=0.26, 3=0.17, 4=0.13, 5=0.06, 6=0.04.

Figure 5. SE flank of Mt. Etna. Activation probability of the vents, as a function of spatial densities (ρ) of historical eruptive fissures and pyroclastic cones, and of proximity to the main weakness zone. Key: 1-6) classes of probability (see text); 7) boundary of the study area – after Crisci et al. [in press], mod.

Table 1. Statistics on lava-flow events at Mt. Etna in the last 400 years (data from Behncke et al., 2005). Historical events are distinguished in classes by duration (in days) and emitted volume of lava (in 10^6 m^3): observed frequencies and, in parentheses, related probability (in %) are listed. In Italics: interpolated values. Asterisks: unrealistic types.

duration \ *volume*	] 0÷32]	] 32÷64]	] 64÷96]	] 96÷128]	] 128÷160]
] 0÷15]	19,0 (20,4)	3,0 (3,2)	*4,2* (*4,5*)	0,0 *	0,0 *
] 15÷30]	6,0 (6,4)	3,0 (3,2)	1,0 (1,1)	*2,3* (*2,5*)	0,0 *
] 30÷60]	3,0 (3,2)	*2,9* (*3,1*)	1,0 (1,1)	*1,3* (*1,4*)	1,0 (1,1)

The model employed for simulating mud flows also belongs to a family of deterministic MCA models [cf. D'Ambrosio et al., 2003a, b] based on the cited algorithm of Di Gregorio and Serra [1999]. In this study, the simplified release $S3_{\text{-}hex}$ of SCIDDICA, first described with reference to a square tessellation by Iovine et al. [2002], was employed. Four elementary processes constitute the transition function σ of $S3_{\text{-}hex}$ [D'Ambrosio et al., 2003a]: σ_1) entrainment of regolith, according to the energy of the flow; σ_2) debris outflows (according to pressure gradients across the cells and to material properties); σ_3) update of debris thickness and energy; σ_4) energy loss and run-up.

Statistics of the May 1998 and December 1999 disasters in Campania, and of the May 2001 and March 2005 events in Calabria, were obtained through interpretation of air-photographs and geologic-geomorphologic field surveying. The amount of regolith available for entrainment was also surveyed in the field, together with other evidence

related to triggering mechanisms, flow development and rheology, erosive character, etc. The "erodability" of the regolith by the flowing masses was empirically estimated by means of visual inspection and appropriate (expeditious) cementation tests. Together with historic information on previous activity, and other geological knowledge, such data allowed us to estimate the characteristics of future phenomena in the same areas. Recent planning instruments (and several unpublished technical reports), produced by local governmental agencies for the same study areas (cf. Figures 6 and 7) in accordance with "emergency" laws (ex DL.180/98, L.267/98, L.226/99, OMI.3029/99), permitted us to imagine a set of likely sources among the sectors exposed to highest landslide potential.

For the two study areas in Campania, calibration was first carried out manually (by trial and error) on a standard platform by employing the fitness function e_1, and later refined with GA. The 1998 Curti mud flow on the southern slope of Pizzo d'Alvano and the 1999 Vallicelle mud flow on the northern slope of Mt. Pizzone were taken as reference cases. Validation was performed against similar mud-flows that occurred during the same disasters in the vicinity of the reference cases [cf. Iovine et al., 2003a, b]. In Calabria, the mud-flow events triggered on the northern slope of Mt. Serro Indice, which stroke the hamlet of Favazzina on 12 May 2001 and 31 March 2005, were selected for calibration and subsequent cross validation. Calibration was first performed manually, and only later by means of sequential GA (again, by employing the fitness function e_1). Incidentally, an improved release of the model (S_{4c}), which is substantially similar to *S3*$_{\text{-}hex}$, was employed for this study area – for details on the model, see D'Ambrosio et al. [2007].

As for lava-flow susceptibility/hazard analyses, a regular grid of hundreds of "possible" sources, located at ca. 50 m intervals along the uppermost border of each hazardous sector, was assumed. For each source, a statistically-significant number of simulations was planned by adopting appropriate combinations of source extent and model parameters. These were selected on the basis of geomorphologic/historical knowledge, statistics of past events, and of calibration results (cf. Table 2). Accordingly, a scenario of soil-slip activation (and related mud-flows), which is comparable with the recentmost disasters occurred in the same areas, was assumed. Nevertheless, as detailed historical and field analyses of past events are still in progress, to date only simplified susceptibility maps could be produced. Therefore, a rather limited number of sources were hypothesized within sectors exposed to highest hazard, using available literature and administrative plans. In particular, a sub-set of n.12 sources was selected for each of the Campanian study areas [Iovine et al., 2003a, b], corresponding to locations with the highest probability of soil-slip triggering - as shown in the maps created after the 1998 and 1999 disasters by Caruso et al. [2005], and by the Basin Authority of the rivers Liri, Garigliano and Volturno [2000], respectively (cf. Figure 6). A regularly spaced set of sources was instead selected for the Calabrian study area, along the uppermost unstable sectors of the slopes, as classified in the "Plan of Hydro-geological Asset" (PAI) landslide maps of Bagnara Calabra, Scilla and Favazzina (cf. Figure 7) by the Calabrian Basin Authority [2001]. In all these cases, source extents were chosen according to a precautionary principle, by selecting maximum values per each combination of slope angle and elevation, from available statistics of past events.

Finally, mudflow susceptibility maps were constructed through GIS overlapping and successive frequency classification, by following (roughly) the same approach as described above for lava flows; resulting frequencies were mapped through grey- or colour-scales.

For each study area, required information for the application of the models (*fv* or *S3*$_{\text{-}hex}$) were arranged as input matrices of hexagonal cells, containing: 1) elevation data (*fv* and *S3*$_{\text{-}hex}$); 2) thickness of erodable regolith (only for *S3*$_{\text{-}hex}$); 3) location and extent of the vent/s (*fv*) or landslide source/s (*S3*$_{\text{-}hex}$); and 4) real events (*fv* and *S3*$_{\text{-}hex}$). Model parameters were initialised by considering the characteristics of events to be simulated, in addition to implementation constraints. For the model *fv*, the parameters are: p_a) cell apothem; p_s) duration of a CA step; p_{Tv}) temperature of lava at the vent; p_{Ts}) temperature of lava at stopping; p_{adv}) adherence at the vent; p_{ads}) adherence at stopping; p_{cool}) cooling parameter. For *S3*$_{\text{-}hex}$, the parameters are: p_a) cell apothem; p_{adh}) adherence; p_f) threshold for outflows; p_r) relaxation rate; p_{ri}) run-up loss; p_{mt}) threshold for erosion; p_{pef}) erosion factor. In Table 2, "optimal" values obtained through calibration are listed.

In all the performed experiments, mud and lava flows were simulated one at a time, results being only later superimposed in the GIS. In other experiments (here not described), flows were allowed to start together, in order to appreciate their mutual interference.

Table 2. Parameters and optimal values for the models *fv* (on the left), after Crisci et al. [in press], and *S3-hex* (on the right), after Iovine et al. [2003a, b]. In the last column, double values refer to the Pizzo d'Alvano (left) and Vallicelle (right) study areas.

parameter	*measure*	*opt. value*
p_a	m	5
p_s	s	155.29
p_{Tv}	K	1373
p_{Ts}	K	1165.35
p_{adv}	m	0.7
p_{ads}	m	12
p_{cool}	$m \cdot t^{-1} \cdot K^{-3}$	$2.9 \cdot 10^{-14}$

parameter	*measure*	*opt. value*	
p_a	m	1.25	
p_{adh}	m	0.001	
p_f	m	0.1	
p_r	-	1	
p_{rl}	m	0.6	1.5
p_{mt}	m^2	3.5	2.0
p_{pef}	-	0.015	0.065

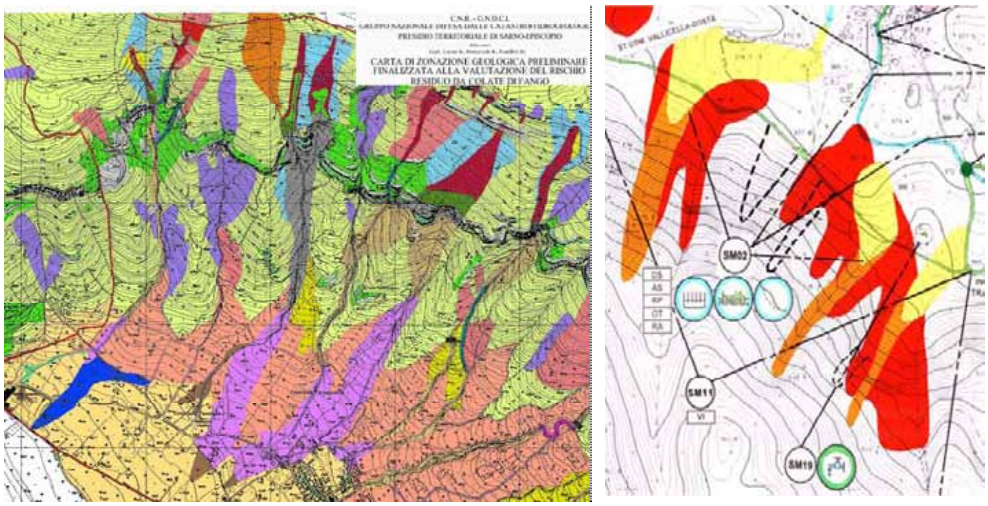

Figure 6. a) On the left, extract of the "Mudflow residual risk map" of the southern slope of Mt. Pizzo d'Alvano. Highest probabilities of soil-slip activation are shown in red tones, orange, dark-violet and in light-blue. Bare rock outcrops are in green, while zones exposed to mud-flow deposition are in light violet and dark-pink - after Caruso et al. [2005]. b) On the right, extract of the "Plan for Removal of the Highest Risk Conditions" of the northern slope of Mt. Pizzone. Highest landslide risk levels are in red, while mud-flows that occurred in December 1999 are either in orange (source-track) or in yellow (deposition zone) - after Basin Authority of the rivers Liri, Garigliano and Volturno [2000].

Figure 7. Extracts of the "Hydro-geological Setting Plan" (PAI) for Scilla (left), Favazzina (middle), and Bagnara Calabra (right). Key: red or black polygons delimit recent/active or dormant/inactive landslides, respectively; dashed polygons delimit landslide-zones; blue lines follow main drainages. Landslide types are distinguished by means of symbols inside (V: slide, U: flow) – after Calabrian Basin Authority [2001].

4. RESULTS

Examples of lava-flow susceptibility and hazard map for the SE flank of Mt. Etna (based on the cited sub-sample of n.1056 simulations) are shown in Figure 8. In the susceptibility map, the main drainages appear mostly exposed to invasion from lava flows, which may originate within the assumed "source zone" (cf. Figures 4 and 5) - a rather similar result may be obtained by merely evidencing the drainages on a contour map. Most of the poorly-exposed area, between Zafferana and Trecastagni, is presently diffusely urbanized. In contrast, in the hazard map highest hazard values are limited to the NW portion of the study area – i.e. at highest elevation a.s.l., and closer to the right flank of the DSGD.

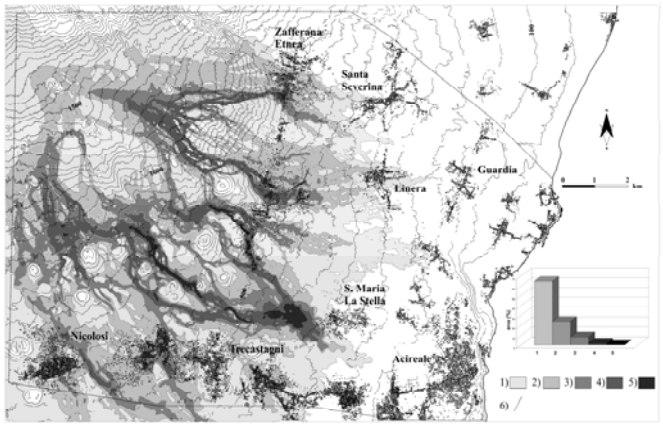

In the susceptibility map (on the left), sites not affected by any simulation amount to ca. 41.5% of the considered area. At the other extreme, the maximum number of simulations affecting a given site is 952. The histogram shows area percentages with respect to the overall affected sites, per each class of relative susceptibility.

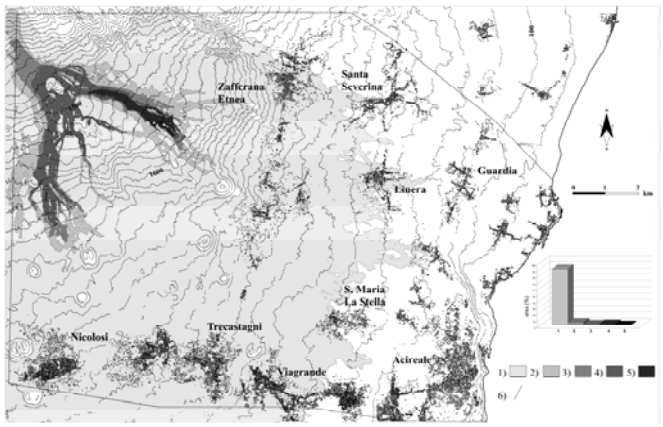

The hazard map (on the left) is based on the same set of simulations employed for elaborating the susceptibility map shown above. The histogram shows the percentages, with respect to the overall affected area, per each class of relative hazard (values: 90.3, 5.2, 1.7, 2.4, and 0.5, respectively).

Figure 8. SE flank of Mt. Etna. Lava-flow susceptibility map (a, on top), and hazard map (b, on bottom). Key: 1-5) classes of relative susceptibility/hazard (see text); 6) boundary of the study area - after Crisci et al. [in press], mod.

Figure 9 shows examples of mud-flow susceptibility zonation for the Vallicelle and the southern slope of Pizzo d'Alvano Massif. The zones affected by one/more simulated phenomena are distinguished by means of different colours. Depending also on location of selected sources, some of the drainages appear to be mostly exposed to mud-flow events. At the base of the massifs, the sectors characterized by the worst conditions coincide fairly well with those severely stricken during the recent 1998 and 1999 disasters.

Figure 10 illustrates examples of mud-flow susceptibility zonation in proximity of Bagnara Calabra, Favazzina and Scilla, along the Tyrrhenian coast of Calabria [La Manna, in prep.]. Also in these maps, zones affected by a different number of simulated events are shown by means of red-tones. In this case, the sectors which appear to be most exposed to flow-invasion are mainly located along the main drainages and the coastal plain. Many of the simulated cases directly affect the urbanized areas as well as threaten the existing infrastructures - as actually occurred in several of the historical events.

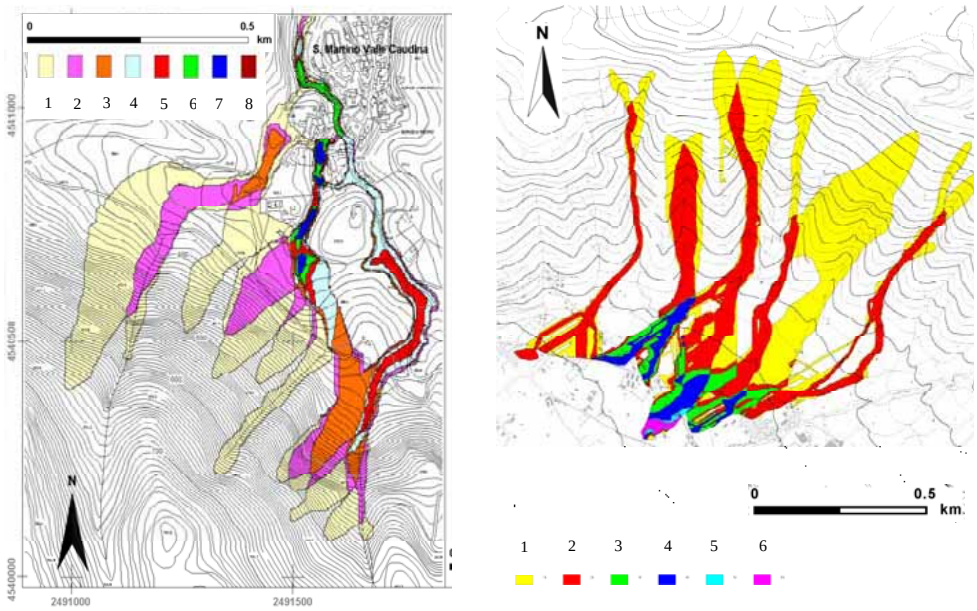

Figure 9. Preliminary mud-flow susceptibility maps for the study areas of: a) Vallicelle area (on left), and b) southern slope of Pizzo d'Alvano Massif (on right). The number of simulated cases which affect a given sector is graphically shown with different colours (ranging from 1 to either 6 or 8, according to the legends on bottom of the maps).

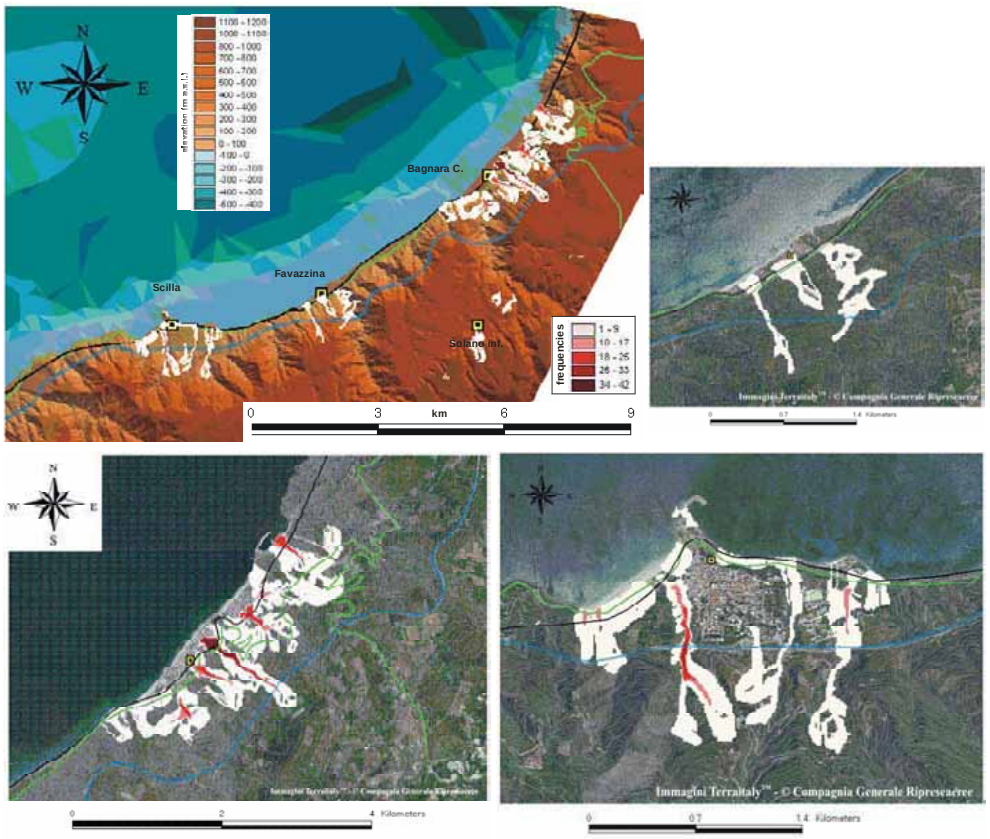

Figure 10. Preliminary mud-flow susceptibility maps for the Calabrian study area (only the sectors in proximity of the villages of Bagnara Calabra, Favazzina and Scilla were analysed). On the top-left, overall view of the study area; elevation ranges are shown by brown-blue tones. Blow-ups: Bagnara Calabra (bottom, left), Favazzina (top-right) and Scilla (bottom right). In all the maps, the number of events (frequency) affecting each zone is shown by means of red-tones (cf. legend in the overall map). Black, blue and green lines mark the railway, the highway, and the state road SS.18, respectively.

5. CONCLUSIONS

The methodological approach for mud-flow and lava-flow susceptibility/hazard mapping, briefly illustrated by examples in the present paper, is based on CA-modelling and GIS-analyses, combined with geological *l.s.* knowledge and historical information in order to empirically assign probabilities to the events of each considered scenario. Source locations and characteristics of the simulated events (e.g. source size for soil slips, effusion functions for vents) were in fact selected also on the basis of statistics of past events that occurred in the same study areas. By storing the performed simulation into a GIS environment and by successively overlapping and weighting the simulations (based on criteria which may be refined in time), the zonation of the study areas into sectors variously exposed to the considered dangers resulted to be a quite fast and effective task.
The CA-modelling approach surmounted several difficulties, which commonly hamper classic numerical methods. Its inherent limits, stemming from the necessity of a "discrete" description of the phenomena, are indeed well balanced by other appealing strong points. Among the greatest advantages of CA: they have the great capability to derive high performance from parallel computers: they are quite robust and do not generally show instability problems; they can fully incorporate even very-dense DEMs.
In the examples described, two simplified releases of CA-models were employed. A number of real cases – that occurred in the same study areas or within similar settings – were employed for calibration and validation (greatly facilitated by use of GA). Incidentally, a strongly innovative derivation of the model for mudflows (FLOW-S*) is presently undergoing final tests and calibration against real cases (data from both field real cases, and flume experiments performed at the CNR-IRPI laboratory). This new release is by far more physically-based with respect to previous ones. It is inspired by the well-known "equivalent fluid" approach, adapted to the discrete space-time CA viewpoint, and is characterized by a subset of physical parameters, which can be tuned depending on the material actually involved in the flow [cf. Iovine & Mangraviti, 2008]. Similarly, a more "physical" version of the model for lava flows is being derived, aiming at better capturing some specific behaviours of the considered real cases (e.g. tunnelling). Finally, thanks to parallel GA, libraries of parameters for both the models are presently being implemented by considering a set of "representative" types of study cases. This should provide a faster implementation of the described approach even to other (but comparable) areas of interest.
The above-presented preliminary results of mud-flow and lava-flow susceptibility/hazard maps, although based only on a sub-set of the overall planned simulations, clearly depict the most hazardous sectors of the considered study areas. The same zones were the most severely affected by the recent disasters that occurred in the past ten years.

ACKNOWLEDGMENTS

The approach described has been fine-tuned in the past ten years within a framework of multidisciplinary cooperation among researchers of the Italian National Research Council and colleagues of different universities. Unpublished, preliminary results for the Calabrian study area, anticipated herein, are being developed by Stefano La Manna for his degree thesis at the University of Calabria (under the direction of G. Iovine, V. Lupiano and R. Rongo). All the GIS elaborations were performed by V. Lupiano. Extracts of orthophotos of the Calabrian coast belong to the 1998 flight "Immagini Terraitaly™", courtesy of Compagnia Generale Ripreseaeree S.p.A., Parma (www.terraitaly.it).

REFERENCES

Acocella, V., and M. Neri, What makes flank eruptions? The 2001 Etna eruption and its possible triggering mechanisms. *Bulletin of Volcanology*, *65*, 517-529, 2003.

Basin Authority of the rivers Liri, Garigliano and Volturno, Plan for Removal of the Highest Risk Conditions – Map of the areas exposed to highest landslide risk levels, Tav.4.2 in scale 1/5,000 (*in Italian*), Technical Report, Genio Civile di Avellino, 2000.

Behncke, B., M. Neri, and A. Nagay, Lava flow hazard at Mount Etna (Italy): New data from a GIS-based study. In: Manga, M., Ventura, G. (Eds.), Kinematics and dynamics of lava flows. *Geological Society of America Special Paper*, *396*, 189-208, 2005.

Borgia, A., L. Ferrari, and G. Pasquarè, Importance of gravitational spreading in the tectonic and volcanic evolution of Mount Etna. *Nature*, *357*, 231-235, 1992.

Calabrian Basin Authority, Hydro-geological Setting Plan (PAI) (*in Italian*), Regione Calabria, Councillorship for Public Works, Catanzaro, 2001 - available on line at http://www.autoritadibacinocalabria.it/PAI/Home/html/Pai_home.htm

Caruso, A., R. Monteverde, and L.M. Puzzilli, Preliminary geological zonation map for the evaluation of the residual mud-flow risk (in scale 1,5000). CNR-GNDCI, Presidio Territoriale di Sarno-Episcopio (*in Italian*), Technical Report. In: Cascini, L., D. Guida, and G. Sorbino, The territorial presidium, a field experience, Chapter 6, Rubettino, Soveria Mannelli, *GNDCI publ. 2857*(B), 2005 - available on-line at http://www.commissario2994.it/originali/Zonazione_Episcopio.jpg

Corazzato, C., and A. Tibaldi, Fracture control on type, morphology and distribution of parasitic volcanic cones: an example from Mt. Etna, Italy. *Journal of Volcanology and Geothermal Research*, *158*, 177-194, 2006.

Crisci, G.M., S. Di Gregorio, and G.A. Ranieri, A cellular space model of basaltic lava flow. In: Mesnard, G. (Ed.), Proc. Int. AMSE Conf. on Modelling and Simulation, *11*, 65-67, AMSE, Paris, 1982.

Crisci, G.M., R. Rongo, S. Di Gregorio, and W. Spataro, The simulation model SCIARA: the 1991 and 2001 lava flows at Mount Etna, *Journal of Volcanology and Geothermal Research*, *132*, 253–267, 2004.

Crisci, G.M., G. Iovine, S. Di Gregorio, and V. Lupiano, Lava-flow hazard on the SE flank of Mt. Etna (Southern Italy), *Journal of Volcanology and Geothermal Research*, in press.

D'Ambrosio, D., S. Di Gregorio, S. Gabriele, and R. Gaudio, A Cellular Automata model for soil erosion by water, *Physics and Chemistry of the Earth*, *26*(B), 33-40, 2001.

D'Ambrosio, D., S. Di Gregorio, and G. Iovine, Simulating debris flows through a hexagonal Cellular Automata model: Sciddica $S_{3\text{-}hex}$. *Natural Hazards and Earth System Sciences*, *3*, 545–559, 2003a.

D'Ambrosio, D., S. Di Gregorio, G. Iovine, V. Lupiano, R. Rongo, and W. Spataro, First simulations of the Sarno debris flows through Cellular Automata modelling, *Geomorphology*, *54*, 91-117, 2003b.

D'Ambrosio, D., Rongo, R., Spataro, W., Avolio, M.V., Lupiano, V., Lava invasion susceptibility hazard mapping through cellular automata. In: El Yacoubi, S., B. Chopard, and S. Bandini (Eds.), ACRI 2006, LNCS *4173*, 452-461, 2006.

D'Ambrosio, D., G. Iovine, W. Spataro, and H. Miyamoto, A macroscopic collisional model for debris-flows simulation, *Environmental Modelling and Software*, *22*(10), 1417-1436, 2007.

Del Prete, M., F.M. Guadagno, and A.B. Hawkins, Preliminary report on the landslides of 5 May 1998, Campania, southern Italy, *Bulletin of Engineering Geology and Environment*, *57*, 113–129, 1998.

Di Gregorio, S., and R. Serra, An empirical method for modelling and simulating some complex macroscopic phenomena by cellular automata, *Future Generation Computer Systems*, *16*, 259–271, 1999.

Hungr, O., A model for the runout analysis of rapid flow slides, debris flows, and avalanches. *Canadian Geotechnical Journal*, *32*, 610-623, 1995.

Iovine G., S. Di Gregorio, D. D'Ambrosio, and V. Lupiano, Debris Flows and Cellular Automata: an example of simulation from the 1998 disaster of Sarno (Italy). In: Delahaye D., F. Levoy, and O. Maquaire (Eds.), Geomorphology: from expert opinion to modelling. A tribute to Professor Jean-Claude Flageollet. Proc. Int. Symp. "Geomorphology: from expert opinion to modelling", Strasbourg, 26-27 April 2002, SODIMPAL, Rouen, 55-64, 2002.

Iovine, G., and S. Di Gregorio, Simulating mud flows by means of Cellular Automata: considerations on the model SCIDDICA (release S2) (*in Italian*). *Bollettino della Società Geologica Italiana*, *122*, 63-84, 2003.

Iovine, G., S. Di Gregorio, and V. Lupiano, Assessing debris-flow susceptibility through cellular automata modelling: an example from the May 1998 disaster at Pizzo d'Alvano (Campania, Southern Italy). In: Rickenmann, D., Chen, C.L. (Eds.), Proc. 3rd Int. Conf.

on Debris-Flow Hazards Mitigation: Mechanics, Prediction, and Assessment, Davos, Switzerland, 1. Millpress, Rotterdam, 623–634, 2003a.

Iovine, G., S. Di Gregorio, and V. Lupiano, Debris-flow susceptibility assessment through cellular automata modeling: an example from the 15-16 December 1999 disaster at Cervinara and San Martino Valle Caudina (Campania, southern Italy). *Natural Hazards and Earth System Sciences 3*, 457–468, 2003b.

Iovine, G., S. Di Gregorio, D. D'Ambrosio, V. Lupiano, L. Merenda and G. Nardi, Evaluating and mapping mud-flow susceptibility by applying a Cellular Automata model (*in Italian*). In: Proc. "Mudflow risk mitigation at Sarno and other villages affected by the May 1998 disaster". Napoli, 2-3 May 2005, 175-185, 2007.

Iovine G., and P. Mangraviti, The model FLOW-S* for flow-type landslides. Preliminary considerations on model performances. Proc. AOGS 5th Annual General Meeting, 16-20 June, Busan-Korea, Abstract Volume in CD-ROM, 2008.

Iverson, R.M., The physics of debris flows, *Reviews in Geophysics*, *35*, 245-296, 1997.

Iverson, R.M., S.P. Schilling, and J.W. Vallance, Objective delineation of lahar-inundation hazard zones, *Geological Society of America Bulletin*, *110*(8), 972-984, 1998.

La Manna, S., Mudflow susceptibility mapping through CA-modelling and GIS-techniques along the southern Tyrrhenian coast of Calabria – The sector between Scilla and Bagnara Calabra. Degree thesis at the University of Calabria, in prep.

McBirney, A.R., and T. Murase, Rheological properties of magmas, *Annual Review of Earth Planetary Sciences*, *12*, 337–357, 1984.

Miyamoto, H., and S. Sasaki, Simulating lava flows by an improved cellular automata method, *Computers & Geosciences*, *23*, 283-292, 1997.

Murray, A.B., and C. Paola, A cellular model of braided rivers, *Nature*, *371*, 54-57, 1994.

Pitman, E.B., A. Patra, A. Bauer, M.F. Sheridan, and M. Bursik, Modeling and Computing Geophysical Mass Flows. In: Hou, T., and E. Tadmor (Eds.), Hyperbolic Problems: Theory, Numerics, Applications, Springer, New York, 807-818, 2003.

Romano, R., and C. Sturiale, The historical eruptions of Mt. Etna (volcanological data). *Memorie della Società Geologica Italiana*, *23*, 75-97, 1982.

Sorriso-Valvo, G.M., and C. Tansi, Large-scale landslides and deep-seated gravitational slope deformations in Calabria (*in Italian*). Geografia Fisica e Dinamica Quaternaria, *19*, 395-408, 1996.

Succi, S., The Lattice Boltzmann Equation for Fluid Dynamics and Beyond. Oxford University Press, pp.368, Oxford USA, 2004.

Tortorici L., C. Monaco, C. Tansi, and O. Cocina, Recent and active tectonics in the Calabrian arc (Southern Italy). *Tectonophysics*, *243*, 37-55, 1995.

United Nations, Mudflows. Experience and Lessons Learned from the Management of Major Disasters. Department of Humanitarian Affairs, U.N., Geneva, 1997.

Vittori, E., F. Fumanti, D. Ligato, and A. Triglia, Technical report on the surveying in the area affected by the hydrogeological crisis of 15–16 December 1999 in the Caudina Valley (Avellino) (*in Italian*), ANPA and ARPA Campania, 14 January, 2000.

APPENDIX

A) The "minimisation algorithm of differences" [after Di Gregorio and Serra, 1999]

At step t, two quantities are identified in the central cell: the fixed part $q(0)$ and the mobile part p of its height. The mobile part can be distributed to the adjacent cells (e.g. thickness of landslide debris or lava flow); the fixed part cannot change during the simulation (e.g. elevation related to the unerodable bedrock). The height of the central cell is given by the sum of two terms $p+q(0)$. The height of the i^{-th} adjacent cell of the neighbourhood is: $q(i)$, $1 \le i \le m-1$. At step $t+1$, the outflow from the central cell to the i^{-th} neighbouring cell is denoted by $f(i)$, $0 \le i \le m$, where $f(0)$ is the part of p which is not distributed. Let $q_0(i)=q(i)+f(i)$, $0 \le i \le m-1$ be the sum of the content of a neighbouring cell (at step t), plus the flow coming from the central cell, and let $q_{0\min}$ be the minimum value for $q_0(i)$. The determination of the outflows from the central cell to the adjacent cells is based on the local minimisation of the differences in "height", as described by the following expression:

$$\sum_{i=0}^{m-1}(q'(i) - q'_{\min}) \qquad (1)$$

B) The model S_{3-hex} [after D'Ambrosio et al., 2003]

Formally, it is: $S_{3-hex} = \langle R, X, Q, P, \sigma \rangle$, where

- $R=\{(x,y)\in Z^2 \mid -l_x \le x \le l_x, -l_y \le y \le l_y\}$ is the cellular space, where Z is the set of integers.
- X={central, NNW, NNE, E, SSE, SSW, W} is the neighbourhood, given by the "central" cell and its six adjacent cells.
- $Q=Q_a \times Q_{th} \times Q_e \times Q_d \times Q^6_o$ is the finite set of states of the *finite automaton*, given by the Cartesian product of the sets of the considered substates: Q_a = average cell elevation a.s.l. (bedrock + regolith); Q_{th} = thickness of landslide debris; Q_e = energy of landslide debris; Q_d = depth of erodable regolith; Q_o = debris outflow from the central cell toward any cell of the neighbourhood. The value of the substate x in the cell is expressed by $q_x \in Q_x$.
- $P=\{p_a, p_t, p_{adh}, p_f, p_r, p_{rl}, p_{mt}, p_{er}\}$ is the set of the model parameters (cf. Table 2).
- $\sigma=Q^7 \to Q$ is the transition function, constituted by the elementary processes $\sigma_1, \sigma_2, \sigma_3, \sigma_4$.
- σ_1: $Q_a \times Q_e \times Q_{th} \times Q_d \times p_{er} \times p_{mt} \to Q_a \times Q_e \times Q_{th} \times Q_d$ is the process of "entrainment". The erosion condition is: $q_e(0) > p_{mt}$. If $\Delta_d < q_d(0)$, the eroded quantity of regolith is $\Delta_d = (q_e(0) - p_{mt}) p_{er}$, else $\Delta_d = q_d(0)$.
- σ_2: $Q^7_a \times Q^7_{th} \times Q_e \times p_{adh} \times p_r \times p_f \to Q^6_o$ is the process of "debris outflows".
- σ_3: $(Q_{th} \times Q_e \times Q^6_o)^7 \to Q_{th} \times Q_e$ is the process of "update" of debris thickness (q_{th}) and energy (q_e).
- σ_4: $Q_e \times Q_{th} \times p_{rl} \to Q_e$ is the process of "energy loss and run-up". It is modelled, by reducing the run-up (r) to a value – not lower than $q_{th}(0)$ – by the parameter p_{rl}. If $[k \cdot q_e(0)/q_{th}(0) - p_{rl}] > q_{th}(0)$, the loss of run-up is $\Delta_r = p_{rl}$, else $\Delta_r = k \cdot q_e(0)/q_{th}(0) - q_{th}(0)$, where $k=2/\rho g A$, ρ=density of the material, g=gravitational acceleration, A=area of the cell.

C) The model *fv* [after Crisci et al., 2004]

Formally, it is: $fv = \langle R, L, X, Q, P, \sigma, \Gamma \rangle$, where

- R and X = see above.
- $L \subset R$=specifies the vents.
- $Q=Q_a \times Q_t \times Q_T \times Q_f^6$ is the finite set of states of the *finite automaton*, given by the Cartesian product of the sets of the considered substates: Q_a is the average cell elevation a.s.l.; Q_t is the thickness of lava in the cell; Q_T is the average lava temperature in the cell; Q_f^6 is the lava outflow from the central cell toward any cell of the neighbourhood.
- $P = \{ p_a, p_s, p_{Tv}, p_{Ts}, p_{adv}, p_{ads}, p_{cool} \}$ is the set of the model parameters (cf. Table 2).
- $\sigma = Q^7 \to Q$ is the transition function, constituted by the elementary processes $\sigma_1, \sigma_2, \sigma_3$.
- σ_1: is the process of "lava outflows". The minimisation algorithm of differences (see above) is applied to the amount of lava exceeding the adherence (v), i.e. the aliquot of lava which remains in the cell, due to viscosity. It is:

$$v = k_1 e^{-k_2 T} \tag{2}$$

in which $T \in Q_T$ is the lava temperature; k_1 and k_2 depend on lava rheological properties and are computed as follows:

$$\begin{cases} p_{adv} = k_1 e^{-k_2 p_{Tv}} \\ p_{ads} = k_1 e^{-k_2 p_{Ts}} \end{cases} \tag{3}$$

- σ_2: is the process of "variation of lava temperature". It is computed by means of a two-step procedure, as temperature can change due either to a) mixing of masses at different temperatures, or b) surface radiation. Accordingly, in the first step:

$$T_{av} = \left(t_r \times T(0) + \sum_{i=1}^{6} f(i,0) \times T(i) \right) \Big/ \left(t_r + \sum_{i=1}^{6} f(i,0) \right) \tag{4}$$

is the weighted average temperature of the residual lava inside the cell plus the lava inflows from neighbouring cells, where $t_r \in Q_t$ is the residual lava thickness inside the central cell (after outflows distribution), $T \in Q_T$ is the lava temperature, and $f(i,0)$ is the lava inflow from the i^{th} neighbouring cell (as computed by the minimisation algorithm).
In the second step, the loss of thermal energy due to surface radiation is computed as:

$$T = T_{av} \Big/ \sqrt[3]{1 + \left(T_{av}^3 C \Delta t A / V \right)} \tag{5}$$

where $C=p_{cool}$ depends on lava rheology, $\Delta t = p_s$, A is the exposed area of the lava, and V the lava volume.

- σ_3: is the process of "lava halting". If the temperature of the lava inside the cell drops below a given threshold, p_{Ts}, the mass of lava comes to a halt, due to an increase of viscosity, thus becoming part of the topography. The elevation of the cell is increased by an amount equal to lava thickness, and lava thickness is set to zero.
- $\Gamma = \{ \gamma_1, \gamma_2, \ldots \gamma_i \ldots \gamma_v \}$ is the set of effusion-rate functions assigned to the vents, where v is the number of considered vents, and $\gamma_i : Q_t \times \mathbf{N} \to Q_t$ is the effusion-rate function (in time), which specifies the amount of lava emitted from the i^{-th} vent during the simulation (expressed in terms of thickness, in meters) at each step $s \in \mathbf{N}$, with $\mathbf{N}$ = set of natural numbers.